第 50 卷 第 9 期/2023 年 5 月/中国激光 研究论文

中国激光

一种椎弓根螺钉内固定术中非同源低重叠率点云的配准方法

张立静[1,2]，王斌斌[1,2]，王玮[3]，武博[1,2*]，张楠[1,2]

[1]首都医科大学生物医学工程学院，北京 100069；

[2]首都医科大学临床生物力学应用基础研究北京市重点实验室，北京 100069；

[3]首都医科大学宣武医院骨科，北京 100053

摘要 在手术导航系统辅助的椎弓根螺钉内固定术中，术前与术中点云配准精度是影响导航定位效果的重要因素。由于术前与术中点云的获取方式不同，且术中暴露位置受限，两种非同源三维点云存在初始位姿差异大、重叠率低的问题，现有的配准算法在术前术中点云配准时容易失效且精度不高。为此，本文提出了一种椎弓根螺钉内固定术中非同源低重叠率点云的配准方法。首先，对术中点云进行降采样，对术前点云进行基于最远点采样的局部区域划分，选取其中的最优局部区域，与术中点云进行采样一致性初始配准；之后，采用迭代最近点算法进行进一步优化，实现点云的准确对齐。在本文所用数据集上，所提算法在术前术中点云配准实验中的平均旋转误差为0.406°，平移误差为0.474 mm，实现了初始位姿差异大、重叠率低的非同源术前术中点云的高精度配准，与现有算法相比，配准成功率从66.67%提高至100%。

关键词 医用光学；椎弓根螺钉内固定术；非同源点云；初始位姿差异大；低重叠率；点云配准

中图分类号 TP391.41 **文献标志码** A **DOI**：10.3788/CJL230561

1 引 言

在脊柱手术中，椎弓根螺钉内固定术主要用来固定病变椎体，是保持脊柱稳定的重要手术方法[1]。椎弓根螺钉置入不当，会极大概率产生严重的手术并发症[2]。而手术导航的使用，可以为医生提供精准定位，消除人为操作失误，提高椎弓根螺钉内固定术的准确性与安全性。手术导航越来越多地被应用到各种临床手术中，辅助外科医生进行微创手术和提前规划路径，从而提高手术质量并缩短手术时间[3]。

目前，点云配准已在多个领域[4-6]被广泛应用，在手术导航系统中也是重要的技术之一[7]，其目标是实现患者所在空间与术前影像空间的准确对齐，其中配准的精度是影响导航系统准确性的重要因素。点云配准的应用包括但不限于：1)神经外科导航系统的配准研究[8]。为提高配准精度，通常采用最小二乘投影算法，在图像空间中生成与患者空间点云匹配的最佳点云，再进行迭代最近点(ICP)配准。在体模实验中，最小二乘投影算法的表面配准误差和目标配准误差均有所改善。2)辅助椎弓根螺钉置入术[9]。术中通常使用结构光扫描仪获取点云，采用改进的共面四点配准方法将获取的点云与术前重建点云进行配准，二者具有较高的配准精度。3)经皮腹腔穿刺手术导航[10]。术中腹部点云由结构光扫描仪获取，并以CT图像作为约束清除无关区域点，再基于高斯混合模型的相干点漂移算法对术前、术中点云进行配准，具有较高的精度和效率。4)机器人辅助长骨截骨手术[11]。粗配准依靠固定在手术部位处跟踪刚体上的基准点来完成，再采用基于距离自适应的改进ICP算法进行精配准，配准误差始终优于基于ICP的配准方法。点云配准方法在辅助脊柱手术导航实现术前术中点云精确配准时存在两个主要问题：1)由于术前术中两点云由不同的成像设备获取，存在点密度差，且两点云的位姿差异较大；2)术中扫描时患者腰椎的解剖部位暴露受限，再加上周围软组织的遮挡，感兴趣区域仅为有限的局部区域，导致术中点云与术前数据重叠率较低，直接应用现有的配准方法[12-15]实现配准存在一定困难。

针对手术导航系统辅助的椎弓根螺钉内固定术中点云配准存在的上述问题，笔者提出了基于最远点采样的非同源低重叠率术前与术中点云配准算法。

收稿日期：2023-02-22；**修回日期**：2023-03-01；**录用日期**：2023-03-03；**网络首发日期**：2023-03-15

基金项目：国家自然科学基金(61672362)

通信作者：*wubogo@ccmu.edu.cn

2　基于最远点采样的非同源低重叠率术前术中点云配准算法

2.1　算法框架

对于手术导航系统辅助的椎弓根螺钉置入术，术中精准实施手术规划路径的重要前提是术前点云与实际术中位姿点云对齐。其中，术前三维点云是对患者CT影像中的腰椎进行三维重建获得的，术中点云则是使用结构光扫描仪对患者术中暴露部位进行扫描获得的。术前与术中点云存在密度差异大、初始位姿差异大和重叠率低的问题，增加了配准难度。为了解决术前与术中点云的配准问题，笔者提出了基于最远点采样的非同源低重叠率点云配准算法，算法的整体框架如图1所示。

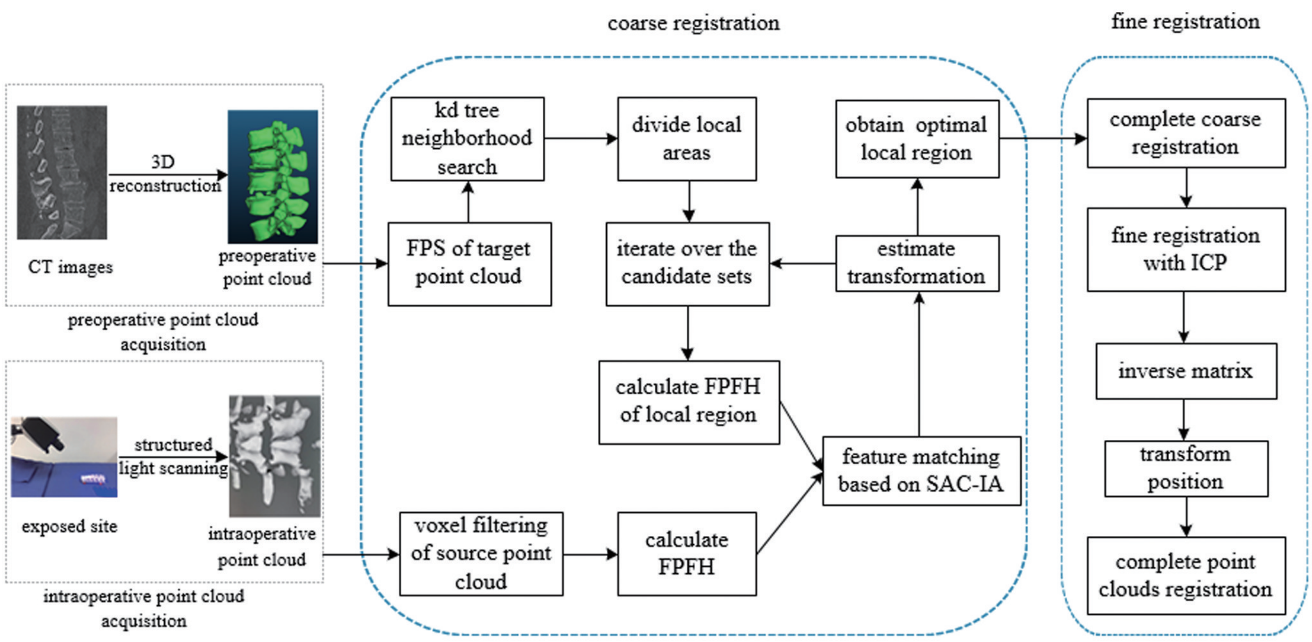

图1　基于最远点采样的非同源低重叠率术前与术中点云配准算法框架

Fig. 1　Framework for preoperative and intraoperative point clouds registration with cross-source and low overlapping based on farthest point sampling

所提出的术前与术中点云配准算法分为粗配准和精配准两部分。粗配准过程如下：1)采用体素滤波算法对术中点云进行降采样，使之与术前点云密度相近。体素滤波算法在点云分布空间创建三维体素栅格，用体素重心点代替体素内的所有点，体素栅格的大小由术前CT影像扫描分辨率确定。2)提取滤波后术中点云的快速点特征直方图(FPFH)特征。对于术前点云，采用最远点采样(FPS)算法进行采样，基于采样点采用kd树算法将术前点云划分为多个局部区域，局部区域组成候选集合。3)遍历候选集合，计算局部区域的FPFH特征，采用采样一致性初始配准算法(SAC-IA)对术中点云进行特征匹配和位姿变换估计，比较术中点云与局部区域特征匹配的距离误差，误差最小时对应的局部区域为最优局部区域，其对应的变换为术中点云与术前点云粗配准的变换。通过最远点采样算法与SAC-IA算法实现最优局部区域与术中点云的配准，从而使得点云在较大初始位姿差异和低重叠率情况下也能较好地对齐。

最后，在粗配准的基础上进行精配准，将最优局部区域的点云作为目标点云，采用ICP精配准算法将术中点云与目标点云进一步对齐，得到优化的变换矩阵，再对矩阵取逆，对术前点云作位姿变换，即可完成术前到术中三维点云的配准。

2.2　基于最远点采样的局部区域获取

本文采用最远点采样算法[16]进行局部区域的获取，如图2所示。首先采用最远点采样算法对术前点云Q进行采样，在术前点云上得到一组足够分散且均匀的采样点Q'，如图2(a)所示。最远点采样的思想是通过不断迭代选择距离已有采样点集合最远的点，算法流程如下：

1) 在输入点云中选择一个点p_0作为起始点，得到采样点集合$Q'=\{p_0\}$；

2) 计算所有点到p_0点的距离，选择最大值对应的点为p_1，更新采样点集合为$Q'=\{p_0,p_1\}$；

3) 计算输入点云中每个点p_i到集合Q'的距离，即计算点p_i到集合Q'中每个点的距离，取最近距离为点p_i到Q'的距离$d(p_i,Q')$；

4) 选择距离$d(p_i,Q')$中最大值对应的点为p_2，更新采样点集合为$Q'=\{p_0,p_1,p_2\}$；

5) 重复步骤3)、步骤4)，直至采样点数量为n时终止，此时采样点集合为$Q'=\{p_0,p_1,\cdots,p_n\}$。

之后将采样点$\{p_0, p_1, \cdots, p_n\}$作为中心点，基于kd树对采样点进行邻域搜索，生成局部区域，n个局部区域构成候选集合，如图2(b)所示，其中的编号为采样点与局部邻域的对应情况。对于采样点云中的每个点p_i，设置搜索半径为r，其对应的三维区域$P(p_i)$可表示为

$$P(p_i)=\left\{p|p\in Q,\ p_i\in Q',\ \|p_i-p\|\leqslant r\right\}。\quad (1)$$

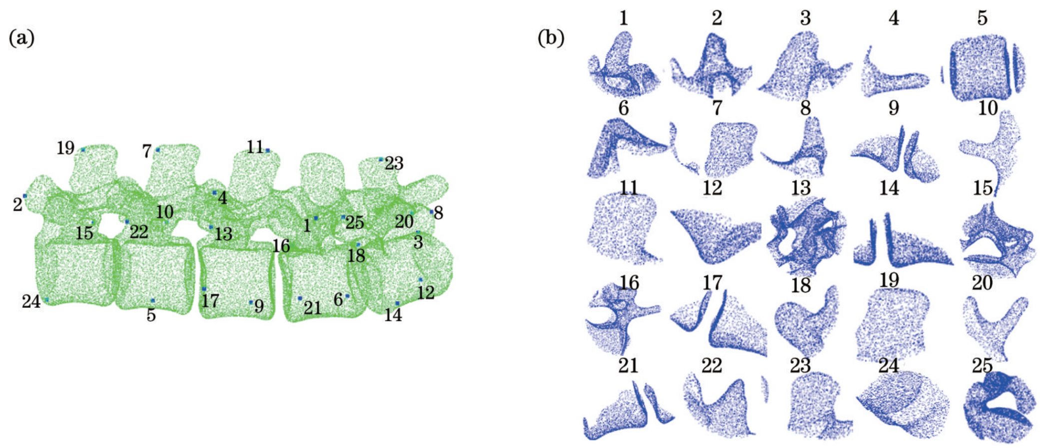

图2　腰椎点云的采样点及其对应的局部区域。(a)采样点分布；(b)采样点对应的局部区域

Fig. 2　Sampling points of lumbar point cloud and their corresponding local regions. (a) Distribution of sampling points; (b) local regions corresponding to the sampling points

生成的多个局部邻域可以覆盖整个模型。为了避免目标位置不包含在候选集合中，需要采样足够多的点。采样点数n取决于术中点云和术前点云中点的数量，其计算公式为

$$n=\left\lceil\frac{n_{\mathrm{TP}}}{n_{\mathrm{SP}}}\right\rceil,\quad (2)$$

式中：n_{TP}为术前点云TP包含的点数；n_{SP}为预处理后术中点云SP包含的点数；$\lceil\ \rceil$表示对结果向上取整。为了保证相似性搜索的有效性，搜索半径r设置为术中点云最长轴的长度。r值的计算公式为

$$r=\sqrt{(\boldsymbol{T}_{\max}-\boldsymbol{T}_{\min})^2},\quad (3)$$

式中：$\boldsymbol{T}_{\max}$、$\boldsymbol{T}_{\min}$分别为术前点云TP中最长轴两个端点的三维坐标。

2.3　基于最优局部区域的点云配准

最优局部区域与术中点云配准采用SAC-IA配准算法，即：遍历候选集合获取最优局部区域，得到粗配准变换，然后基于ICP的精细化算法实现最终变换。为获取最优局部区域，利用术中点云和术前局部区域及对应的FPFH特征，采用SAC-IA进行初始变换。首先，随机选取$m(m\geqslant 3)$个点，保证选取的点与点之间的距离大于设置的最小距离；对于每个点，通过最近邻搜索在目标点云中查找与源点云FPFH特征具有相似特征的k个点，随机选择一个点作为对应点，形成m组对应的点对；利用点的对应关系得到局部区域点云与术中点云之间的变换矩阵，再采用Huber损失函数[17]计算变换后的源点云与目标点云之间的距离误差，记为$E(H)$。$E(H)$的定义为

$$E(H)=\sum_{i=1}^{n}H(e_i),\quad (4)$$

式中：e_i为点云中对应点对之间的距离，其中对应点对为变换后源点云中的点与目标点云中与之对应的最近邻点；$H(e_i)$为第i个对应点对的距离误差度量。$H(e_i)$的计算公式为

$$H(e_i)=\begin{cases}\dfrac{1}{2}e_i^2, & \|e_i\|\leqslant l_{\mathrm{e}}\\ \dfrac{1}{2}l_{\mathrm{e}}\left(2\|e_i\|-l_{\mathrm{e}}\right), & \|e_i\|>l_{\mathrm{e}}\end{cases},\quad (5)$$

式中：l_{e}为距离误差阈值。遍历候选集合，比较每个局部区域块作为目标点云时的距离误差，即

$$\{E;\ T\}=\min\left\{E_1(H), E_2(H), \cdots, E_N(H)\right\},\quad (6)$$

式中：N是划分局部区域的数量。将距离误差$E(H)$最小的局部区域为最优局部区域，其对应的变换为术中点云与术前点云粗配准的最优变换，对术中点云施加粗配准最优变换矩阵，实现粗匹配，为后续精配准提供良好的初始位姿。

精配准采用ICP精细化配准方法，将最优局部区域的点云作为目标点云，将其与粗配准后的术中点云对齐。优化目标函数为

$$\{\boldsymbol{R};\ \boldsymbol{t}\}=\underset{\{\boldsymbol{R};\ \boldsymbol{t}\}}{\arg\min}\sum_{i=1}^{n_{\mathrm{p}}}\left\|\boldsymbol{T}^i-\boldsymbol{R}\cdot\boldsymbol{S}^i-\boldsymbol{t}\right\|^2,\quad (7)$$

式中：$\boldsymbol{T}^i$、$\boldsymbol{S}^i$是术前点云与术中点云中的一对对应点的三维坐标；n_{p}是对应点对的数量；$\boldsymbol{R}$为最优旋转变换矩阵；$\boldsymbol{t}$为最优平移变换矩阵。选取术前点云和术中点云距离最近的对应点，迭代产生使目标函数最小的最优旋转变换矩阵$\boldsymbol{R}$与平移变换矩阵$\boldsymbol{t}$，对变换矩阵$\{\boldsymbol{R};\ \boldsymbol{t}\}$取逆，即可实现手术过程中术前点云与术中点云的精确配准。

3　实验结果与分析

为评估本文算法对非同源低重叠率点云配准的性能，在腰椎术前与术中点云上进行实验。FPFH描述子的描述性较好，计算时间快，而SHOT描述子具有较强的鲁棒性，因此，将本文算法与基于FPFH特征的ICP配准方法[18]（FPFH+ICP）、基于SHOT特征的ICP配准方法[19]（SHOT+ICP）进行比较。实验所用计算机处理器为Intel（R） Core（TM） i7-8550U CPU @ 1.80 GHz 1.99 GHz。

3.1　实验数据

本文术前术中点云配准实验所用腰椎CT数据来自SpineWeb数据集[20-21]和首都医科大学某临床医院。将SpineWeb数据集设为来源Ⅰ，首都医科大学某临床医院设为来源Ⅱ。首先采集患者术前CT影像数据，重建出完整的人体腰椎三维点云模型。对于术中点云，由于无法获得真实的手术场景，所以对术前影像重建的三维点云进行3D打印，使用蔡司COMET6结构光扫描仪扫描打印模型（可在满足扫描精度的同时保证扫描效率），并按保留平均目标点误差为0.003 mm的扫描点对扫描仪进行设置，以模拟实际手术过程中的操作；对术中暴露位置进行扫描，获得患者手术过程中的空间点云。本文共进行了9次术前与术中点云配准实验，术前点云数据编号、术中暴露部位、点云重叠率及初始位姿差异如表1所示。

表1　术中点云与术前点云重叠率及初始位姿差异

Table 1　Overlapping ratio and location difference between intraoperative and preoperative point clouds

Data	Exposed site	Overlapping ratio μ /%	Source	Rotation /(°)			Translation /mm		
				X	Y	Z	X	Y	Z
001	L1	1.73	Ⅰ	99.35	46.63	86.79	74.86	−28.85	20.40
001	L2	1.69	Ⅰ	148.53	48.47	138.47	114.08	−64.99	−103.52
002	L2	1.97	Ⅰ	−87.05	−55.12	106.08	53.53	−47.08	29.48
002	L3	2.29	Ⅰ	109.48	28.19	79.30	−55.67	7.23	40.84
003	L1	1.35	Ⅱ	−76.59	68.13	−88.32	−98.28	−59.36	26.07
004	L1	2.69	Ⅱ	104.67	70.86	97.17	398.10	34.14	19.08
005	L3	1.80	Ⅱ	96.70	42.06	92.16	216.39	−44.52	76.20
006	L1	1.67	Ⅱ	96.94	22.41	82.55	−89.11	45.34	42.65
007	L1	1.66	Ⅱ	89.39	58.15	82.35	−57.78	−42.73	38.71

重叠率μ通过计算源点云SP与目标点云TP的交并比得到，计算公式为

$$\mu=\frac{n_{\mathrm{TP}}\cap n_{\mathrm{SP}}}{n_{\mathrm{TP}}\cup n_{\mathrm{SP}}},\tag{8}$$

式中：$n_{\mathrm{TP}}\cap n_{\mathrm{SP}}$指的是源点云对齐后在目标点云中存在对应点的个数；$n_{\mathrm{TP}}\cup n_{\mathrm{SP}}$为源点云与目标点云并集的点数，由源点云点数与目标点云点数的和减去对应点个数得到。

术前与术中点云的初始位姿差异如表1中旋转角度列与位移列所示，由配准金标准变换矩阵$\boldsymbol{T}^{\mathrm{G}}$计算得到。由于术前点云与术中点云属于非同源点云，两点云间的配准没有明确的$\boldsymbol{T}^{\mathrm{G}}$，所以根据文献[22]所提方法获取术前术中点云配准的金标准变换矩阵$\boldsymbol{T}^{\mathrm{G}}$。首先人工标记三对及以上对应点，对点云进行初始对齐，再采用ICP算法进一步对手动配准结果进行优化得到$\boldsymbol{T}^{\mathrm{G}}$。

3.2　评价指标

接下来对配准误差和配准算法的运行时间进行评估。通过比较粗-精配准变换矩阵$\boldsymbol{T}$与金标准变换矩阵$\boldsymbol{T}^{\mathrm{G}}$，计算旋转误差$e^{\mathrm{r}}$和平移误差$e^{\mathrm{t}}$，计算公式[23]为

$$\begin{cases}e^{\mathrm{r}}=\arccos\left[\dfrac{\mathrm{tr}(\Delta\boldsymbol{R})-1}{2}\right],\\ e^{\mathrm{t}}=\|\Delta\boldsymbol{t}\|\end{cases}\tag{9}$$

其中，

$$\Delta\boldsymbol{T}=\boldsymbol{T}(\boldsymbol{T}^{\mathrm{G}})^{-1}=\begin{bmatrix}\Delta\boldsymbol{R} & \Delta\boldsymbol{t}\\ 0 & 1\end{bmatrix}。\tag{10}$$

3.3　术前与术中点云配准实验

本节对术前点云与术中暴露部位点云进行实验，采用最远点采样算法完成术前点云到术中点云的配准。基于表1所示点云数据，得到了不同重叠率、不同初始位姿下的配准结果，如图3所示。图中所示术中点云为单棘突，术前点云是完整腰椎，第1列是术前点云和术中点云的初始位姿，第2列是术前点云通过最远点采样算法得到的采样点结果，第3列是术中点云与选择的术前最优局部区域的粗配准结果，第4列是精配准结果，第5列是术前点云配准到术中点云的最终结果。

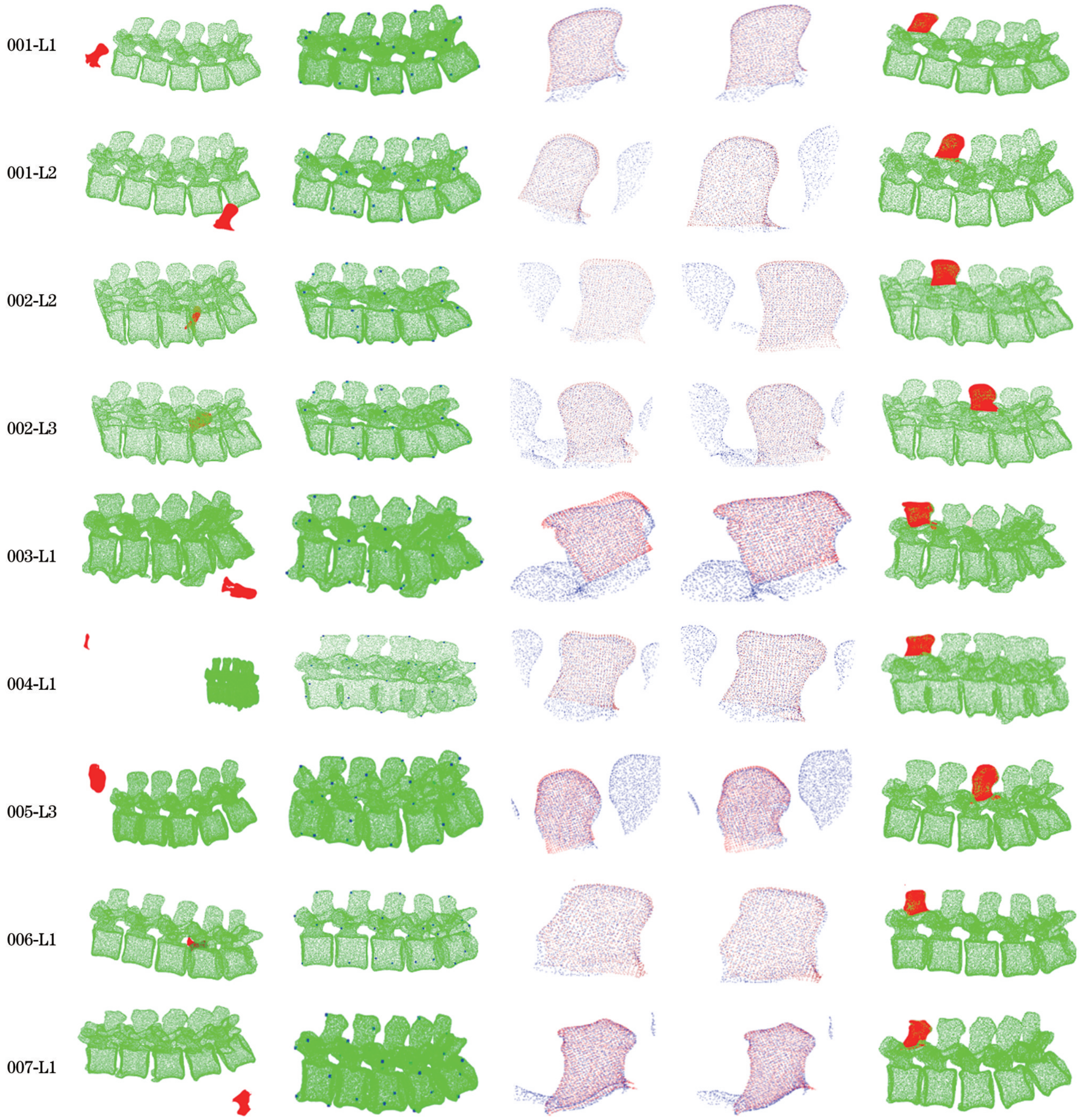

图 3 001-L1、001-L2、002-L2、002-L3、003-L1、004-L1、005-L3、006-L1、007-L1 数据的配准结果

Fig. 3 Registration results of 001-L1, 001-L2, 002-L2, 002-L3, 003-L1, 004-L1, 005-L3, 006-L1, and 007-L1

表 2 比较了术前点云与术中点云在本文算法、FPFH+ICP 算法、SHOT+ICP 算法下的粗/精配准平均误差及运行时间。由实验结果可知，在术前术中点云重叠率低于 3% 的情况下，基于最远点采样的配准算法（本文所提算法）表现最优。当 004、006 数据术中暴露 L1 棘突时，FPFH+ICP 和 SHOT+ICP 两种算法均没有配准成功；当 001 数据术中暴露 L2 棘突时，FPFH+ICP 算法没有配准成功；当 002 数据术中暴露 L3 棘突时，SHOT+ICP 算法不能配准成功，而本文方法可以准确对齐。对于三种算法均能配准成功的术前与术中点云，在 FPFH+ICP 算法下，粗配准平均旋转误差与平均平移误差分别为 20.16°和 32.23 mm；在 SHOT+ICP 算法下，粗配准平均旋转误差与平均平移误差分别为 23.44°和 34.18 mm；而本文所提算法在粗配准时的平均旋转误差与平均平移误差分别为 6.02°和 6.85 mm，且得到的匹配点数最多，为 ICP 精配准提供了更加优异的初始位姿。本文算法精配准的平均旋转误差为 0.406°，平移误差为 0.474 mm，符合临床要求，与其余两种算法的 ICP 配准误差相比有所提升。在运行时间上，与另外两种算法相比，本文算法的运行时间有所增加，但仍保持在 2 min 以内，在实际手术中是可以接受的[24-26]。

表2　术前术中点云粗/精配准误差及运行时间比较

Table 2　Comparison of preoperative and intraoperative point clouds coarse/fine registration errors and running time

Data	Exposed site	Registration algorithm	Coarse registration				Fine registration			
			Matching pairs	e^r /(°)	e^t /mm	Time /s	Matching pairs	e^r /(°)	e^t /mm	Time /s
001	L1	FPFH+ICP[15]	231	35.13	26.52	47.65	1134	0.33	0.38	0.43
		SHOT+ICP[16]	100	19.97	21.54	55.70	1133	0.71	0.66	0.40
		FPS+FPFH+ICP	572	9.27	9.80	117.78	1126	0.34	0.32	0.06
001	L2	FPFH+ICP[15]								
		SHOT+ICP[16]	105	36.45	43.43	58.97	901	0.59	0.78	0.69
		FPS+FPFH+ICP	266	14.81	9.81	92.30	992	0.45	0.32	0.07
002	L2	FPFH+ICP[15]	185	17.62	25.73	43.76	921	0.93	1.21	0.32
		SHOT+ICP[16]	106	44.21	64.30	52.16	915	0.64	0.85	0.56
		FPS+FPFH+ICP	486	4.07	4.76	103.74	743	0.34	0.43	0.06
002	L3	FPFH+ICP[15]	202	8.78	9.86	44.42	1014	1.00	0.41	0.35
		SHOT+ICP[16]								
		FPS+FPFH+ICP	320	8.21	3.54	89.54	1142	0.25	0.85.	0.08
003	L1	FPFH+ICP[15]	163	19.82	40.49	47.01	1683	0.45	0.99	0.54
		SHOT+ICP[16]	150	20.62	35.22	64.90	1677	0.64	1.01	0.52
		FPS+FPFH+ICP	395	8.43	4.84	115.12	1293	0.83	0.44	0.06
004	L1	FPFH+ICP[15]								
		SHOT+ICP[16]								
		FPS+FPFH+ICP	228	7.75	17.82	79.01	990	0.31	0.47	0.05
005	L3	FPFH+ICP[15]	311	25.54	67.23	45.56	1054	0.26	0.93	0.27
		SHOT+ICP[16]	244	29.39	48.02	59.77	1049	0.39	1.54	0.61
		FPS+FPFH+ICP	814	5.54	11.86	95.63	920	0.37	0.64	0.04
006	L1	FPFH+ICP[15]								
		SHOT+ICP[16]								
		FPS+FPFH+ICP	540	4.12	8.51	113.54	818	0.59	0.60	0.07
007	L1	FPFH+ICP[15]	952	2.71	1.16	43.25	1403	0.28	0.27	0.30
		SHOT+ICP[16]	811	3.02	1.81	57.60	1407	0.43	0.58	0.31
		FPS+FPFH+ICP	994	2.79	3.00	108.34	1345	0.13	0.19	0.05

Notes: null indicates that registration fails under the current algorithm.

此外,对上述三种算法的配准成功率进行了比较,结果如表3所示。FPFH+ICP和SHOT+ICP的9次配准实验均成功了6次,而本文所提算法的9次配准实验均成功,配准成功率从对比算法的66.67%提高到了100%。

表3　术前与术中点云配准成功率对比

Table 3　Success rate comparison of preoperative and intraoperative point clouds registration

Algorithm	Number of registration samples	Number of successfully registered samples	Success rate /%
FPFH+ICP[15]	9	6	66.67
SHOT+ICP[16]	9	6	66.67
FPS+FPFH+ICP	9	9	100

4 结 论

对于手术导航系统辅助的椎弓根螺钉内固定术，其配准过程中存在术前和术中两点云初始位姿差异大和重叠率低的问题。针对这一问题，笔者提出了一种基于最远点采样的非同源低重叠率术前术中点云配准算法。对重叠率小于3%的腰椎术前与术中点云进行配准实验，以评估所提算法在重叠率低、初始位姿差异大时的点云配准性能。在本文所用数据集上，所提算法在术前与术中点云配准实验中的平均旋转误差为0.406°，平移误差为0.474 mm，配准成功率为100%，不会使配准结果陷入局部最优。实验结果表明，所提算法对位姿差异大、重叠率低的点云配准具有较高的鲁棒性，可以实现术前点云和术中点云的高精度配准，提高了手术导航的准确性与安全性。不过，所提算法目前仅考虑了术前点云与术中点云的刚性变换，未来拟考虑术前与术中存在的椎间运动，使其更适用于临床。

参 考 文 献

[1] 张同同，王增平，王中华，等. 骨科机器人辅助下脊柱椎弓根螺钉置入准确性与安全性的临床研究[J]. 中国骨伤，2022，35(2): 108-112.
Zhang T T, Wang Z P, Wang Z H, et al. Accuracy and safety of robot assisted pedicle screw placement[J]. China Journal of Orthopaedics and Traumatology, 2022, 35(2): 108-112.

[2] 刘良乐，戴鸣海，董伊隆，等. 胸椎后方不同程度去皮质在椎弓根螺钉置入中的稳定性研究[J]. 中国生物医学工程学报，2017，36(3): 375-379.
Liu L L, Dai M H, Dong Y L, et al. The stability study of thoracic pedicle srew instrumentation with different degrees of posterior cortex bitten away[J]. Chinese Journal of Biomedical Engineering, 2017, 36(3): 375-379.

[3] Choi A, Chae S, Kim T H, et al. A novel patient-to-image surface registration technique for ENT- and neuro-navigation systems: proper point set in patient space[J]. Applied Sciences, 2021, 11(12): 5464.

[4] 靳宇婷，张益华，崔海华，等. 一种基于轮廓特征约束的飞机蒙皮配准方法[J]. 光学学报，2021，41(3): 0312001.
Jin Y T, Zhang Y H, Cui H H, et al. An aircraft skin registration method based on contour feature constraint[J]. Acta Optica Sinica, 2021, 41(3): 0312001.

[5] Arnold E, Mozaffari S, Dianati M. Fast and robust registration of partially overlapping point clouds[J]. IEEE Robotics and Automation Letters, 2022, 7(2): 1502-1509.

[6] 刘如飞，王飞，任红伟，等. 一种利用地理实体目标特征的道路场景激光点云配准方法[J]. 中国激光，2022，49(18): 1810002.
Liu R F, Wang F, Ren H W, et al. Road scene laser point cloud registration method based on geographical object features[J]. Chinese Journal of Lasers, 2022, 49(18): 1810002.

[7] Zheng G Y, Kowal J, González Ballester M A, et al. Registration techniques for computer navigation[J]. Current Orthopaedics, 2007, 21(3): 170-179.

[8] Yoo H, Choi A, Mun J H. Acquisition of point cloud in CT image space to improve accuracy of surface registration: application to neurosurgical navigation system[J]. Journal of Mechanical Science and Technology, 2020, 34(6): 2667-2677.

[9] Zhu S J, Zhao Z, Pan Y W, et al. Markerless robotic pedicle screw placement based on structured light tracking[J]. International Journal of Computer Assisted Radiology and Surgery, 2020, 15(8): 1347-1358.

[10] Li J, Deng Z Q, Shen N Y, et al. A fully automatic surgical registration method for percutaneous abdominal puncture surgical navigation[J]. Computers in Biology and Medicine, 2021, 136: 104663.

[11] Zhang C L, Liu Y, Zhang Y G, et al. A hybrid feature-based patient-to-image registration method for robot-assisted long bone osteotomy[J]. International Journal of Computer Assisted Radiology and Surgery, 2021, 16(9): 1507-1516.

[12] Pan Y, Yang B S, Liang F X, et al. Iterative global similarity points: a robust coarse-to-fine integration solution for pairwise 3D point cloud registration[C]//2018 International Conference on 3D Vision (3DV), September 5-8, 2018, Verona, Italy. New York: IEEE Press, 2018: 180-189.

[13] Koide K, Yokozuka M, Oishi S, et al. Voxelized GICP for fast and accurate 3D point cloud registration[C]//2021 IEEE International Conference on Robotics and Automation (ICRA), May 30-June 5, 2021, Xi'an, China. New York: IEEE Press, 2021: 11054-11059.

[14] 侯彬，金尚忠，王赟，等. 点云配准方法在粗配准中的比较[J]. 激光与光电子学进展，2020，57(8): 081502.
Hou B, Jin S Z, Wang Y, et al. Comparison of point cloud registration methods in coarse registration[J]. Laser & Optoelectronics Progress, 2020, 57(8): 081502.

[15] 杨宜林，李积英，王燕，等. 基于NDT和特征点检测的点云配准算法研究[J]. 激光与光电子学进展，2022，59(8): 0810016.
Yang Y L, Li J Y, Wang Y, et al. Point cloud registration algorithm based on NDT and feature point detection[J]. Laser & Optoelectronics Progress, 2022, 59(8): 0810016.

[16] Qi C R, Yi L, Su H, et al. PointNet++: deep hierarchical feature learning on point sets in a metric space[C]//Proceedings of the 31st International Conference on Neural Information Processing Systems, December 4-9, 2017, Long Beach, California, USA. New York: ACM Press, 2017: 5105-5114.

[17] Rusu R B, Blodow N, Beetz M. Fast point feature histograms (FPFH) for 3D registration[C]//2009 IEEE International Conference on Robotics and Automation, May 12-17, 2009, Kobe, Japan. New York: IEEE Press, 2009: 3212-3217.

[18] Ouyang Z H, Cui S A, Zhang P F, et al. Iterative closest point (ICP) performance comparison using different types of lidar for indoor localization and mapping[J]. Laser in Engineering, 2020, 47(4/5/6): 221-232.

[19] 陆军，邵红旭，王伟，等. 基于关键点特征匹配的点云配准方法[J]. 北京理工大学学报，2020，40(4): 409-415.
Lu J, Shao H X, Wang W, et al. Point cloud registration method based on key point extraction with small overlap[J]. Transactions of Beijing Institute of Technology, 2020, 40(4): 409-415.

[20] Aslan M S, Shalaby A, Farag A A. Clinically desired segmentation method for vertebral bodies[C]//2013 IEEE 10th International Symposium on Biomedical Imaging, April 7-11, 2013, San Francisco, CA, USA. New York: IEEE Press, 2013: 840-843.

[21] Aslan M S, Ali A, Rara H, et al. A novel 3D segmentation of vertebral bones from volumetric CT images using graph cuts[M]//Bebis G, Boyle R, Parvin B, et al. Advances in visual computing. Lecture notes in computer science. Heidelberg: Springer, 2009, 5876: 519-528.

[22] Dong Z, Yang B S, Liang F X, et al. Hierarchical registration of unordered TLS point clouds based on binary shape context descriptor[J]. ISPRS Journal of Photogrammetry and Remote Sensing, 2018, 144: 61-79.

[23] Guo Y L, Sohel F, Bennamoun M, et al. An accurate and robust range image registration algorithm for 3D object modeling[J]. IEEE Transactions on Multimedia, 2014, 16(5): 1377-1390.

[24] Eggers G, Kress B, Rohde S, et al. Intraoperative computed tomography and automated registration for image-guided cranial surgery[J]. Dento Maxillo Facial Radiology, 2009, 38(1): 28-33.

[25] Quang T T, Chen W F, Papay F A, et al. Dynamic, real-time, fiducial-free surgical navigation with integrated multimodal optical imaging[J]. IEEE Photonics Journal, 2020, 13(1): 3900113.

[26] Gueziri H E, Santaguida C, Collins D L. The state-of-the-art in ultrasound-guided spine interventions[J]. Medical Image Analysis, 2020, 65: 101769.

Point Cloud Registration Algorithm with Cross-Source and Low Overlapping Ratio for Pedicle Screw Fixation

Zhang Lijing[1,2], Wang Binbin[1,2], Wang Wei[3], Wu Bo[1,2*], Zhang Nan[1,2]

[1]*School of Biomedical Engineering, Capital Medical University, Beijing* 100069, *China*;

[2]*Beijing Key Laboratory of Fundamental Research on Biomechanics in Clinical Application, Capital Medical University, Beijing* 100069, *China*;

[3]*Department of Orthopedics, Xuanwu Hospital Capital Medical University, Beijing* 100053, *China*

Abstract

Objective In surgical navigation system-assisted pedicle screw fixation, preoperative and intraoperative point clouds registration accuracy is crucial for positioning and navigation. When the patient's preoperative space is accurately registered to the actual surgical space, the surgical instrument can be guided to the patient's surgical site, and the planned surgical path can be accurately implemented during the operation. The preoperative point cloud is obtained by reconstructing the patients' preoperative CT, while a structural light scanner obtains the intraoperative point cloud during the operation. The acquisition methods of two-point clouds differ; hence, their densities and initial poses are quite different. Therefore, they are cross-source point clouds. Moreover, the scanned intraoperative point cloud is a small part of an entire spine since the exposed spine is very limited during an operation. Hence, the overlapping ratio of the preoperative and intraoperative point clouds is low. Existing registration algorithms are prone to fail or derive a low accuracy in preoperative and intraoperative point cloud registration. To solve these problems, this study proposes a preoperative and intraoperative point clouds registration algorithm with cross-source and a small overlapping ratio for pedicle screw fixation.

Methods This study proposes a preoperative and intraoperative point clouds registration algorithm with cross-source and low overlapping ratio based on Farthest Point Sampling (FPS). The proposed algorithm includes coarse and fine registration. The coarse registration comprises three steps. Firstly, the voxel filter was used to down-sample the intraoperative point cloud to bring its density close to the preoperative point cloud. Secondly, the Fast Point Feature Histogram (FPFH) features of the intraoperative point cloud were extracted. The FPS was used to sample the preoperative point cloud, and then the preoperative point cloud was divided into several local regions by kd tree algorithm. These local regions formed the candidate set. Thirdly, the candidate set was traversed to calculate the FPFH features of each local region. The Sample Consensus Initial Alignment (SAC-IA) feature matching method was to realize feature matching and pose transformation estimation of intraoperative point cloud. The distance errors deduced by the SAC-IA method between the intraoperative point cloud and local point cloud were compared and the local region with the minimum distance error was selected as the optimal local region. The transformation of the optimal local region was the intraoperative and preoperative points clouds coarse registration's transformation. In fine registration, the Iterative Closest Point (ICP) algorithm was adopted to further align the intraoperative and the preoperative point cloud. It is performed based on the coarse registration result. The optimal local region is used as the target point cloud at this stage. Using the FPS and SAC-IC methods, an optimal local region sampled from the preoperative point cloud is obtained, enabling the point clouds can align under large original pose difference and low overlapping ratio conditions. In fine registration, the ICP algorithm was adopted to further align the intraoperative and the preoperative point clouds. The fine registration was performed based on the coarse registration results. The optimal local region was used as the target point cloud at this stage.

Results and Discussions Based on the FPS method, the preoperative point cloud is divided into several local regions (Fig. 2). An optimal local neighborhood is derived to complete registration with the intraoperative point cloud. This study adopts nine pairs of preoperative and intraoperative point clouds for testing, with different overlapping ratios and initial poses (Table 1). The visualization results of the registration process using the proposed algorithm are shown in Fig. 3, including the initial pose of nine pairs of point clouds, the sampling results of FPS, and the coarse and fine registration results. To evaluate the performance of the proposed algorithm, two state-of-the-art registration algorithms, FPFH＋ICP and SHOT＋ICP, are adopted for comparison (Table 2). The proposed algorithm achieves the minimum coarse registration error, providing better alignment for ICP fine registration. A comparison of the final registration transformation matrix with the ground truth shows that the average rotation error is 0.406° and the translation error is 0.474 mm, which meets clinical requirements. Simultaneously, the registration time of the proposed algorithm is less than 2 min, which is adequate for an operation. In addition, the registration success rates of the three algorithms in the experiment are compared (Table 3). The successfully registered FPFH＋ICP and SHOT＋ICP algorithm samples are 6 out of 9. While for the proposed algorithm, it is 9 out of 9, demonstrating that the registration success rate increased from 66.67％ to 100％.

Conclusions This study proposes a point cloud registration algorithm with cross-source and a low overlapping ratio for pedicle screw fixation. Through the registration of preoperative and intraoperative point clouds of a lumbar vertebra with an overlapping ratio of less than 3%, the experimental results show that the proposed algorithm based on FPS can resolve the problems of density differences, large initial pose differences, and low overlapping ratios in the preoperative and intraoperative point clouds registration of pedicle screw fixation assisted by a surgical navigation system. High precision registration can be realized, improving the accuracy and safety of surgical navigation systems. The research only considers the rigid transformation of preoperative and intraoperative point clouds. Preoperative and intraoperative intervertebral motion will be considered in the future to make the proposed system algorithm more suitable for clinical practice.

Key words medical optics; pedicle screw fixation; cross-source point cloud; large initial pose difference; low overlapping ratio; point cloud registration